Journal of *Marine Science and Engineering*

MDPI

Article

Fault-Tolerant Model Predictive Control for Autonomous Underwater Vehicles Considering Unknown Disturbances

Yimin Chen, Shaowen Hao, Jian Gao, Jiarun Wang and Le Li *

School of Marine Science and Technology, Northwestern Polytechnical University, Xi'an 710072, China; yiminchen@nwpu.edu.cn (Y.C.); swhao@mail.nwpu.edu.cn (S.H.); jiangao@nwpu.edu.cn (J.G.); wangjiarun_1997@163.com (J.W.)

* Correspondence: leli@nwpu.edu.cn

Abstract: This paper presents a fault-tolerant model predictive control approach for cross-rudder autonomous underwater vehicles to achieve heading control, considering rudder stuck faults and unknown disturbances. Specifically, additive faults in the rudders are addressed, and an active fault-tolerant control strategy is employed. Fault models of autonomous underwater vehicles have been established to develop the fault-tolerant control method. In the controller design, the stuck faults of complete rudder failure are incorporated to ensure the heading angle control of the autonomous underwater vehicle in faulty conditions. Furthermore, the fault term is decoupled from the control input, and the decoupled control input, along with corresponding constraints, is incorporated into the model's predictive controller design. This approach facilitates controller reconfiguration, thereby enhancing and optimizing control performance. Simulation results demonstrate that the proposed fault-tolerant model predictive control method can effectively achieve stable navigation and heading adjustment under rudder fault conditions in autonomous underwater vehicles.

Keywords: model predictive control; autonomous underwater vehicles; fault-tolerant control

Academic Editor: Sergei Chernyi

Received: 31 December 2024
Revised: 15 January 2025
Accepted: 17 January 2025
Published: 18 January 2025

Citation: Chen, Y.; Hao, S.; Gao, J.; Wang, J.; Li, L. Fault-Tolerant Model Predictive Control for Autonomous Underwater Vehicles Considering Unknown Disturbances. *J. Mar. Sci. Eng.* **2025**, *13*, 171. https://doi.org/10.3390/jmse13010171

1. Introduction

Autonomous underwater vehicles (AUVs) have become increasingly indispensable in the realm of oceanic exploration and exploitation. The ability to operate independently underwater has revolutionized the way we gather data and perform tasks in the depths of the oceans. As the demand for more efficient and reliable AUVs grows, researchers and engineers around the world are continuously striving to enhance their performance through various means, such as optimizing their structural design, upgrading their hardware components, and refining their software algorithms [1].

The development of fault-tolerant control (FTC) originated in the field of computer system design and gradually introduced control systems, aiming to ensure the preservation of system stability or to minimize the resultant performance degradation in the event of system failure [2,3]. The fault-tolerant control technology for AUVs has improved the reliability and stability of AUVs in complex underwater environments, ensuring that AUVs can maintain high-precision positioning in the event of navigation sensor failures or actuator malfunction, thereby successfully completing various deep-sea missions. Ref. [4] proposes a region tracking fault-tolerant control method based on the backstepping method, considering ocean current disturbance, modelling uncertainty, unknown thruster faults and thruster amplitude, and rate saturation constraints. The dynamic model of the propulsion

system of the fully-actuated AUV has been established in [5], thereby achieving fault-tolerant control of the vehicle. In [6], fault models and fault-tolerant strategies are studied to ensure that collision avoidance paths for unmanned surface vessel (USVs) are generated and tracked in scenarios involving actuator failures. The problem of fault localization and fault-tolerant control in AUVs was studied and verified through deep control simulation of AUVs in [7]. In [8], a brief and robust fault-tolerant control method has been proposed, which enables the AUV to navigate to a safe point even in the event of a serious failure of its propulsion system. The simulation results show that when only a single thruster is working normally, the designed controller drives the AUV to the target point in a spiral-like path. Ref. [9] proposes a fuzzy fault-tolerant control strategy based on proposed possibilistic fuzzy C-means fault diagnosis method, taking into account both ocean current interference and thruster faults.

Recent advancements introduced model predictive control (MPC) for AUVs, enhancing fault tolerance by anticipating and mitigating faults [10]. MPC optimizes control actions based on vehicle dynamics and future behavior, ensuring AUVs maintain course and objectives despite adversity. Ref. [11] introduced a MPC approach utilizing quantum particle swarm optimization and incorporated a pseudo-inverse fault-tolerant control strategy during the control process, thereby empowering the unmanned underwater vehicle (UUV) to manage a controllable fault in the thruster. Considering the driving saturation, ocean current disturbance and thrusters failure, a cascaded dynamic tracking controller is designed to achieve stable trajectory tracking for the human occupied vehicle (HOV) in [12]. In response to the challenges of poor real-time performance and trajectory tracking accuracy of AUVs in complex hydrological environments, earlier studies explored the use of Laguerre functions to enhance the efficiency of multi-parametric predictive control, as demonstrated in [13,14]. Building on these foundational contributions, Ref. [15] applied the Laguerre function in the design of an MPC controller, significantly reducing computational complexity. By designing a dual closed-loops robust MPC controller, the AUV achieved trajectory tracking with uncertain model parameters and external random disturbances in [16,17]. In [18], model-based reinforcement learning is utilized to address foreseeable and unobservable disturbances, while a filtered probabilistic MPC method is proposed to iteratively learn the USV model and an MPC-based policy. Ref. [19] utilizes a quantum-behaved particle swarm algorithm to solve MPC optimization problems, effectively handling the speed jump problem.

In addition, research on other control methods such as visual serving control and sliding model control (SMC) has also been conducted in the study of AUVs. Visual service control is typically applied to the docking or retrieval tasks of AUVs, which is often combined with neural networks [20–22]. This control method typically uses monocular or binocular cameras to capture images of the underwater environment and extracts useful visual information through image processing techniques. This information is used as a feedback signal to control the movement of the underwater vehicle, stabilizing it at the target position or following a predetermined trajectory. Given its intrinsic robustness characteristics, SMC has garnered extensive research attention for numerous FTC systems [23]. The structure of the sliding model controller is reconfigured, thereby achieving fault-tolerant control of the UAV in [24]. A propulsion FTC method is introduced for AUVs, grounded in the sliding mode theory, aimed at mitigating the steady-state error induced by thruster faults [25]. Ref. [26] proposes a fault-tolerant control approach utilizing a passive sliding mode to ensure finite-time stability of the closed-loop system, accommodating actuator faults, parametric uncertainties within the system, and unforeseen external disturbances.

The weight matrix is introduced into the design of the controller to represent the degree of thruster failure in [11]. However, MPC is solely implemented at the UUV kinematic

level, whereas the fault control of the thruster is realized via the application of sliding mode control to the dynamic system. In [27], a robust control method has been proposed to achieve the trajectory tracking of surface vessels. The fault-tolerant control method's stability has been proven and feasibility has been verified through simulation. Nevertheless, bias faults are ignored in the design of MPC controllers. Motivated by the above studies, a heading control fault-tolerant control for fully-actuated cross-rudder AUVs is studied. The rudder stuck fault is transformed into a constraint for the MPC optimization problem, while unknown disturbances are considered in the construction of the dynamic model. The primary contributions presented in this paper are summarized as follows:

- A fully-actuated AUV fault model is established by considering the rudder stuck faults. The auxiliary thrusters compensate for the imbalanced torque caused by the rudder stuck faults, in order to ensure system stability.
- A fault-tolerant MPC method is proposed based on the rudder fault model and fault analysis. Compared to the traditional fault-tolerant controllers, the proposed approach decouples the fault terms by transforming the rudder faults as the system constraints, in order to reduce the fault influences.
- The unknown disturbances are considered in the fault-tolerant controller to ensure system robustness. The heading control of the AUV is effectively achieved in the presence of the unknown disturbances and the rudder-stuck faults.

The rests of this paper are arranged as follows. Section 2 illustrates the kinematic and dynamic models of the cross-rudder AUVs with consideration of the rudder fault conditions. In Section 3, the constraints and control input changes caused by rudder faults are analyzed and the fault-tolerant MPC (FTMPC) controller is designed. Sections 4 and 5 show the simulation results and conclusion, respectively.

2. Dynamic and Fault Model

In this study, the AUV's heave, roll, and pitch have little impact on overall performance. Instead, the horizontal plane position and heading changes are key to task completion. Therefore, this research uses a 3-DOF AUV horizontal motion model to simplify calculations.

The kinematic model and dynamic model of the cross-rudder AUVs with 3-DOF are developed for the motion planner and controller design based on the AUV model proposed in [28]. A fault model considering rudder stuck faults is established and analyzed.

2.1. Kinematic Model

The coordinate system selected in this paper is shown in Figure 1. Two Cartesian reference frames are defined to describe the motion of AUVs: namely the earth-centered inertial frame $O_E - x_E y_E z_E$ and the body-fixed reference frame $O_B - x_B y_B z_B$. In this study, the horizontal motion of the AUV is described, which means that the vertical and roll motions are ignored.

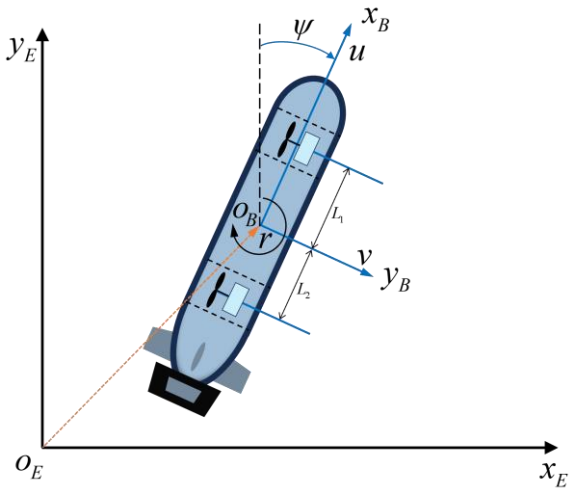

Figure 1. Coordinate system of AUV.

The origin O_E of the earth-centered inertial frame is selected as a reference point on the earth surface. x_E points to an appropriate direction in the horizontal plane. y_E lies in the horizontal plane and perpendicular to the $x_E O_E z_E$ plane. Its orientation makes this frame right-handed.

Considering the fixed-depth sailing scenario, the planner motion is studied in this paper, while the pitch motion and the roll motion are ignored in the motion planning and control. The horizontal motion of the AUV can be described using forward velocity u, lateral velocity v, and angular velocity r. The kinematic model is written as:

$$\dot{\boldsymbol{\eta}} = \boldsymbol{J}(\boldsymbol{\eta})\boldsymbol{v} \tag{1}$$

where the vector $\boldsymbol{\eta} = [x \quad y \quad \psi]^{\mathrm{T}} \in \mathbb{R}^3$ denotes the position and attitude of the AUV in the horizontal plane and the vector $\boldsymbol{v} = [u \quad v \quad r]^{\mathrm{T}} \in \mathbb{R}^3$ denotes the velocity of the AUV. The conversion matrix $\boldsymbol{J}(\boldsymbol{\eta})$ can be described as:

$$\boldsymbol{J}(\boldsymbol{\eta}) = \begin{bmatrix} \cos\psi & -\sin\psi & 0 \\ \sin\psi & \cos\psi & 0 \\ 0 & 0 & 1 \end{bmatrix} \tag{2}$$

2.2. Dynamic Model

The dynamic model is defined in the body-fixed reference frame that is moving and connected with the AUV. The frame chooses the center of buoyancy of the AUV as the origin O_B. x_B runs along the vertical axis of the AUV and points forward. z_B lies in the plane of longitudinal symmetry of the AUV and perpendicular to the x_B and points downward. y_B is located in the lateral symmetry plane and is perpendicular to x_B and z_B, directing to the right from the tail.

A schematic diagram of the AUV mentioned in this paper is shown in Figure 1. It is a fully-actuated underwater vehicle and is equipped with three thrusters in total: one main thruster for forward propulsion and two lateral thrusters for forces and torque in the horizontal plane. l denotes the distances between the cross-section of the cross-rudders and the center of gravity of the AUV, which plays a role as the yaw force arm in subsequent analysis. Considering the unknown disturbances $\boldsymbol{d}$, vehicle equations of motion in directional control can be expressed as follows:

$$\boldsymbol{M}\dot{\boldsymbol{v}} + \boldsymbol{C}(\boldsymbol{v})\boldsymbol{v} + \boldsymbol{D}(\boldsymbol{v})\boldsymbol{v} = \boldsymbol{\tau} + \boldsymbol{d} \tag{3}$$

where

$$\boldsymbol{M} = \mathrm{diag}\left\{ m - X_{\dot{u}} \quad m - Y_{\dot{v}} \quad I_z - N_{\dot{r}} \right\}$$
$$\boldsymbol{C}(\boldsymbol{v}) = \begin{bmatrix} 0 & 0 & -(m - Y_{\dot{v}})v \\ 0 & 0 & (m - X_{\dot{u}})u \\ (m - Y_{\dot{v}})v & -(m - X_{\dot{u}})u & 0 \end{bmatrix}$$
$$\boldsymbol{D}(\boldsymbol{v}) = -\mathrm{diag}\left\{ X_u + X_{|u|u}\left|u\right| \quad Y_v + Y_{|v|v}\left|v\right| \quad N_r + N_{|r|r}\left|r\right| \right\}$$

$\boldsymbol{M}$ is the system inertial matrix, $\boldsymbol{C}(\boldsymbol{v})$ is the Coriolis-centripetal matrix, and $\boldsymbol{D}(\boldsymbol{v})$ denotes the damping matrix. $\boldsymbol{\tau} = [F_X \quad F_Y \quad N]^{\mathrm{T}} \in \mathbb{R}^3$ denotes the total force and torque of the control input. $\boldsymbol{d} = [d_X \quad d_Y \quad d_N]^{\mathrm{T}}$ is the external disturbance vector, where we let there be a positive number $\overline{d} > 0$ satisfying $\|\boldsymbol{d}\| \leq \overline{d}$.

According to the kinematic model Equation (1) and the dynamic model Equation (3), the desired velocity is tracked by the velocity controller, and the force and moment used to control the AUV are obtained using the dynamics model. The perturbation dynamic model is obtained:

$$\begin{aligned} \dot{\boldsymbol{\eta}} &= \boldsymbol{J}(\boldsymbol{\eta})\boldsymbol{v} \\ \dot{\boldsymbol{v}} &= \boldsymbol{M}^{-1}(\boldsymbol{\tau} + \boldsymbol{d} - \boldsymbol{C}(\boldsymbol{v})\boldsymbol{v} - \boldsymbol{D}(\boldsymbol{v})\boldsymbol{v}) \end{aligned} \tag{4}$$

2.3. Modeling and Analysis of Rudder Stuck Faults

The propulsion efficiency of lateral thrusters, which operate perpendicular to the direction of motion, decreases as sailing speed increases, making them more suitable for low-speed AUVs. In contrast, the lift force generated by control surfaces is proportional to the square of the sailing speed and diminishes rapidly at lower speeds, rendering them ideal for high-speed AUV motion control. By complementing each other, rudders and thrusters create a redundant design. In the event of rudder malfunctions, auxiliary thrusters serve as a backup mechanism to maintain the AUV's heading control.

As shown in Figure 2, two auxiliary thrusters, one main thruster, and cross-rudders provide the force and torque required for the AUV's horizontal motion. In this study, the thrust of the AUV is generated by the thrusters (#1–#3) to achieve the surge, sway, and yaw motions, while the yaw moment can be jointly generated by the thrusters and rudders. Due to the symmetrical installation of the cross-rudders, the origin O' of the hull coordinate system in Figure 2 coincides with the center of gravity of the AUV. Meanwhile, the upper and lower surfaces of the vertical rudder are considered as one rudder.

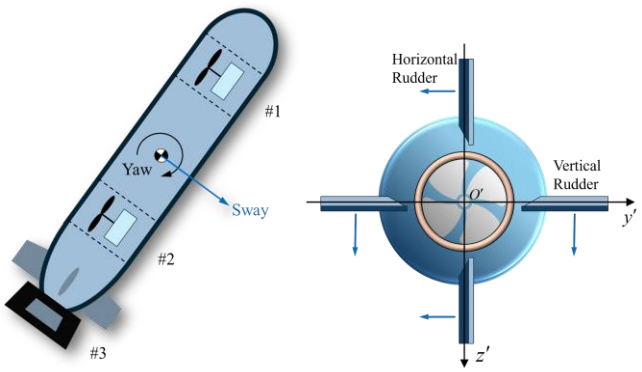

Figure 2. Thrusters and rudders configuration.

The thrust of the auxiliary thrusters is defined by T_1 and T_2, respectively. Define T_3 as the thrust provided by the main thruster. The rudder angle of the vertical rudder

is described by δ_R. The mapping relationship between actuator action vector and AUV control force and torque can be described as

$$\boldsymbol{\tau} = \boldsymbol{B}_{\boldsymbol{\tau}}\boldsymbol{\Theta} \tag{5}$$

where $\boldsymbol{\Theta} = [T_1 \quad T_2 \quad T_3 \quad \delta_R]^{\mathrm{T}} \in \mathbb{R}^4$ is the actuator control action vector. $\boldsymbol{B}_{\tau}$ is defined as the control allocation matrix.

The rudder stuck faults are characterized by conditions where the rudder angle δ_R is stuck at a particular fault angle α. The stuck fault condition is described as

$$\begin{cases} \delta_R = \alpha \\ \delta_{R,\min} \leq \alpha \leq \delta_{R,\max} \end{cases} \tag{6}$$

where $\delta_{R,\min}$ and $\delta_{R,\max}$ denote the maximum and minimum rudder angles of the vertical rudder. The rudder stuck fault model of the AUV actuator is transformed from Equation (5) to

$$\boldsymbol{\tau} = \boldsymbol{\tau}_f + \boldsymbol{\tau}_c = \begin{bmatrix} F_{X,f} & F_{Y,f} & N_f \end{bmatrix}^T + \begin{bmatrix} F_{X,c} & F_{Y,c} & N_c \end{bmatrix}^T \tag{7}$$

where $\boldsymbol{\tau}_f$ and $\boldsymbol{\tau}_c$ are defined as the optimized term and the fault term, respectively. In this study, we assume that the thrust of the main thruster is constant, $T_3 = T_m$. Therefore, $\boldsymbol{\tau}_c$ is the control force generated by the main thruster and faulty rudder. The control force generated by the auxiliary thrusters is denoted as $\boldsymbol{\tau}_f$.

The control force generated by the auxiliary thrusters is denoted as

$$\begin{cases} F_{X,f} = 0 \\ F_{Y,f} = T_1 + T_2 \\ N_f = T_1 L_1 - T_2 L_2 \end{cases} \tag{8}$$

where L_1 and L_2 denote the distances between the auxiliary thrusters and the center of gravity of the AUV. The control forces generated by the main thruster and rudder stuck faults in the fault term are described as follows

$$\begin{cases} F_{X,c} = T_m + X_{uu\delta_R} u^2 \alpha \\ F_{Y,c} = Y_{uu\delta_R} u^2 \alpha \\ N_c = N_{uu\delta_R} u^2 \alpha \end{cases} \tag{9}$$

where $X_{uu\delta_R}$,$Y_{uu\delta_R}$, and $N_{uu\delta_R}$ denote the dimensional coefficients of the force and torque.

Therefore, the fault model is described as

$$\boldsymbol{\tau} = \underbrace{\boldsymbol{B}_{\tau,f}\boldsymbol{\Theta}_f}_{\tau_f} + \underbrace{\boldsymbol{B}_{\tau,c}\boldsymbol{\Theta}_c}_{\tau_c} \tag{10}$$

where $\boldsymbol{\Theta}_f$ and $\boldsymbol{\Theta}_c$ describe the fault term and optimized term and are defined as

$$\begin{cases} \boldsymbol{\Theta}_f = [\ T_1 \quad T_2\ ]^{\mathrm{T}} \in \mathbb{R}^2 \\ \boldsymbol{\Theta}_c = [\ T_3 \quad \delta_R\ ]^{\mathrm{T}} \in \mathbb{R}^2 \end{cases} \tag{11}$$

and the corresponding control allocation matrixes are derived as

$$\boldsymbol{B}_{\tau,f} = \begin{bmatrix} 0 & 0 \\ 1 & 1 \\ L_1 & -L_2 \end{bmatrix} \quad \boldsymbol{B}_{\tau,c} = \begin{bmatrix} 1 & X_{uu\delta_R} u^2 \\ 0 & Y_{uu\delta_R} u^2 \\ 0 & N_{uu\delta_R} u^2 \end{bmatrix} \tag{12}$$

Considering the input saturation of the AUV actuators, the thrust force of each thruster should meet as follows:

$$T_i = \begin{cases} T_{i,\min} & T_i \le T_{i,\min} \\ T_i & T_{i,\min} \le T_i \le T_{i,\max} \\ T_{i,\max} & T_i \ge T_{i,\max} \end{cases}, \quad (i = 1,2,3) \tag{13}$$

where T_i is the thrust of the ith thruster. $T_{i,\min}$ and $T_{i,\max}$ denote the maximum and minimum thrust values of the thrusters. The upper and lower bounds of the actuator action vector are defined as

$$\begin{cases} \boldsymbol{\Theta}_{f,\max} = \begin{bmatrix} T_{1,\max} & T_{2,\max} \end{bmatrix}^{\mathrm{T}} \\ \boldsymbol{\Theta}_{f,\min} = \begin{bmatrix} T_{1,\min} & T_{2,\min} \end{bmatrix}^{\mathrm{T}} \end{cases} \tag{14}$$

Then the constraint set of control efforts under rudder stuck faults is denoted as

$$\boldsymbol{\Xi}_f = \left\{ \boldsymbol{\Theta}_f \in \mathbb{R}^2, \boldsymbol{\Theta}_{f,\min} \le \boldsymbol{\Theta}_f \le \boldsymbol{\Theta}_{f,\max} \right\} \tag{15}$$

3. Fault Tolerant Control

This study focuses on an AUV equipped with three thrusters, enabling three degrees of freedom in horizontal motion. In practical applications, thruster failures can arise due to various factors, leading to changes in thrust vector alignment and input constraint sets. By analyzing and assessing the force distribution and rudder dynamics, the proposed controller addresses potential faults, optimizing the AUV's propulsion and steering capabilities to maintain robust operational performance.

In this section, the actuator faults are transformed into controller constraints and a fault-tolerant MPC controller for the cross-rudder AUV is constructed as in Figure 3.

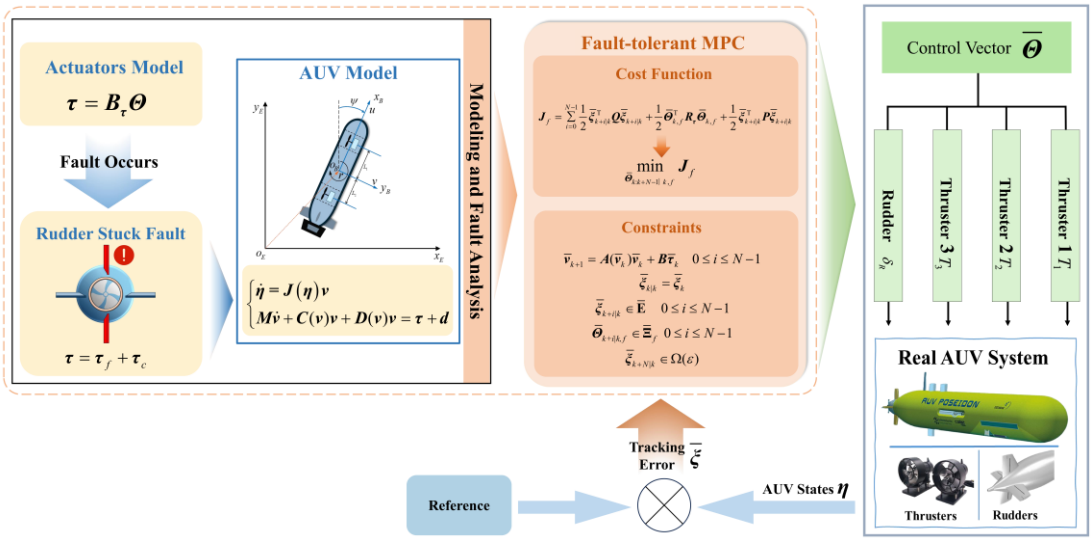

Figure 3. AUV control block diagram.

3.1. MPC Controller Design

In this section, the MPC is developed for controller design of the AUV. In Section 2.2, the 3-DOF dynamic model of a fully-actuated autonomous underwater vehicle is given by

$$\boldsymbol{M}\dot{\boldsymbol{v}} + \boldsymbol{C}(\boldsymbol{v})\boldsymbol{v} + \boldsymbol{D}(\boldsymbol{v})\boldsymbol{v} = \boldsymbol{\tau} + \boldsymbol{d}$$

The input constraint set is defined as $\mathbf{U}$ such that $\boldsymbol{\tau} \in \mathbf{U}$. The discrete time dynamic model with a sampling period T can be derived by using the Newton–Euler method as

$$\begin{aligned} \boldsymbol{v}_{k+1} &= \boldsymbol{v}_k + T\boldsymbol{M}^{-1}(-\boldsymbol{C}(\boldsymbol{v}_k)\boldsymbol{v}_k - \boldsymbol{D}(\boldsymbol{v}_k)\boldsymbol{v}_k + \boldsymbol{\tau}_k + \boldsymbol{d}_k) \\ &= \boldsymbol{A}(\boldsymbol{v}_k)\boldsymbol{v}_k + \boldsymbol{B}\boldsymbol{\tau}_k + \boldsymbol{w}_k \end{aligned} \tag{16}$$

where $\boldsymbol{A}(\boldsymbol{v}_k) = \boldsymbol{I} - T\boldsymbol{M}^{-1}(\boldsymbol{c}(\boldsymbol{v}_k)+\boldsymbol{D}(\boldsymbol{v}_k))$ and $\boldsymbol{B} = T\boldsymbol{M}^{-1}$. $\boldsymbol{w}_k = T\boldsymbol{M}^{-1}\boldsymbol{d}_k$ denotes the disturbance at time instant k, and it is bounded by the disturbance set $\mathbf{W}$, i.e., $\boldsymbol{w}_k \in \mathbf{W}$. $\boldsymbol{\tau}_k = \boldsymbol{B}_{\boldsymbol{\tau}}(\boldsymbol{v}_k)\boldsymbol{\Theta}_k$, and $\boldsymbol{\Theta}_k$ is the action vector at time k.

The nominal velocity model is established as a solution without considering disturbance:

$$\overline{\boldsymbol{v}}_{k+1} = \boldsymbol{A}(\overline{\boldsymbol{v}}_k)\overline{\boldsymbol{v}}_k + \boldsymbol{B}\overline{\boldsymbol{\tau}}_k \tag{17}$$

Let $\boldsymbol{v}_d$ be the desired velocity vector and define $\overline{\boldsymbol{\xi}}_k = \overline{\boldsymbol{v}}_k - \boldsymbol{v}_d$ as the velocity tracking error. $\overline{\boldsymbol{\tau}}_k = \boldsymbol{B}_{\boldsymbol{\tau}}\overline{\boldsymbol{\Theta}}_k$ is the nominal control input which is the solution to a nominal optimal control problem to be designed later. $\overline{\boldsymbol{\Theta}}_k$ is contained within a limited set of actions, i.e., $\overline{\boldsymbol{\Theta}}_k \in \overline{\boldsymbol{\Xi}}_k$, and $\overline{\boldsymbol{\Xi}}_k$ will be defined later.

We assume that $(\boldsymbol{A}, \boldsymbol{B})$ is stabilizable, then there exists a feedback gain matrix $\boldsymbol{K}$ such that $\boldsymbol{A}_{\boldsymbol{K}} = \boldsymbol{A} + \boldsymbol{B}\boldsymbol{K}$ is Hurwitz. The actual feedback control law is designed as

$$\boldsymbol{\tau}_k = \overline{\boldsymbol{\tau}}_k + \boldsymbol{K}\boldsymbol{e}_k \tag{18}$$

where $\boldsymbol{e}_k = \boldsymbol{\xi}_k - \overline{\boldsymbol{\xi}}_k$ is the difference between the actual and nominal tracking error, whose state equation satisfies

$$\boldsymbol{e}_{k+1} = \boldsymbol{A}_{\boldsymbol{K}}\boldsymbol{e}_k + \boldsymbol{w}_k \tag{19}$$

Since $\boldsymbol{A}_{\boldsymbol{K}}$ is Hurwitz, $\boldsymbol{e}_k$ will be constrained within a robust invariant set. The minimal disturbance invariant set is given by

$$\boldsymbol{S}_K(\infty) = \sum_{i=0}^{\infty} \boldsymbol{A}_{\boldsymbol{K}}^i \mathbf{W} \tag{20}$$

Here, $\sum$ denotes set addition. Therefore, the feedback control law ensures the actual error state trajectory evolves in a tube centered on the nominal error state trajectory. If the nominal error system (17) is asymptotically stable, then the actual tracking error will be ultimately bounded, and the size of the residual set is determined by the minimal disturbance invariant set.

In the following, the nominal control input $\overline{\boldsymbol{u}}_k$ is designed by formulating and solving a receding horizon constrained optimization problem based on Equation (17). This approach optimizes performance within the prediction horizon while ensuring compliance with system constraints. To ensure robust satisfaction, the original input and state constraints are tightened as follows

$$\begin{aligned} \overline{\mathbf{E}} &= \mathbf{E} - \mathbf{S}_K(\infty) \\ \overline{\mathbf{U}} &= \mathbf{U} - K\mathbf{S}_K(\infty) \end{aligned} \tag{21}$$

where the original error set is defined as $\mathbf{E}$.

A well-known result is first recalled.

Lemma 1. *For the system (17), given two positive definite matrices $\boldsymbol{Q}$ and $\boldsymbol{R}$, there exists a constant $\varepsilon > 0$ such that:*

1. *The level set $\boldsymbol{\Omega}(\varepsilon) \triangleq \left\{ \overline{\boldsymbol{\xi}} \middle| V_f(\overline{\boldsymbol{\xi}}) \leq \varepsilon^2 \right\} \subset \overline{\mathbf{E}}$ is a control invariant set with the control law $\overline{\boldsymbol{\tau}}_k = \boldsymbol{K}_f\boldsymbol{\xi}_k \in \overline{\mathbf{U}}$;*
2. *For any $\boldsymbol{\xi}_k \in \boldsymbol{\Omega}(\varepsilon)$ the following equality holds*

$$V_f(\boldsymbol{A}_{\boldsymbol{K}_f}\overline{\boldsymbol{\xi}}) - V_f(\overline{\boldsymbol{\xi}}) = -\frac{1}{2}\overline{\boldsymbol{\xi}}^{\mathrm{T}}\boldsymbol{Q}_{\boldsymbol{K}_f}\overline{\boldsymbol{\xi}} \tag{22}$$

where $\boldsymbol{K}_f = -\left(\boldsymbol{B}^{\mathrm{T}}\boldsymbol{P}\boldsymbol{B}+\boldsymbol{R}\right)^{-1}\boldsymbol{B}^{\mathrm{T}}\boldsymbol{P}\boldsymbol{A}$, $\boldsymbol{P}$ *is the unique solution to the discrete algebraic Riccati equation*

$$\boldsymbol{P} = {\boldsymbol{A}_{\boldsymbol{K}_f}}^{\mathrm{T}} P \boldsymbol{A}_{\boldsymbol{K}_f} + \boldsymbol{Q}_{\boldsymbol{K}_f} \tag{23}$$

and

$$\begin{cases} V_f(\overline{\boldsymbol{\xi}}) = \frac{1}{2}\overline{\boldsymbol{\xi}}^{\mathrm{T}}\boldsymbol{P}\overline{\boldsymbol{\xi}} \\ \boldsymbol{A}_{\boldsymbol{K}_f} = \boldsymbol{A} + \boldsymbol{B}\boldsymbol{K}_f \\ \boldsymbol{Q}_{\boldsymbol{K}_f} = \boldsymbol{Q} + {\boldsymbol{K}_f}^{\mathrm{T}}\boldsymbol{R}\boldsymbol{K}_f \end{cases}$$

To minimize tracking error, the cost function $\boldsymbol{J}$ of MPC controller is defined as follows

$$\boldsymbol{J} = \sum_{i=0}^{N-1} \frac{1}{2}\overline{\boldsymbol{\xi}}_{k+i|k}^{\mathrm{T}}\boldsymbol{Q}\overline{\boldsymbol{\xi}}_{k+i|k} + \frac{1}{2}\overline{\boldsymbol{\tau}}_{k+i|k}^{\mathrm{T}}\boldsymbol{R}\overline{\boldsymbol{\tau}}_{k+i|k} + \frac{1}{2}\overline{\boldsymbol{\xi}}_{k+N|k}^{\mathrm{T}}\boldsymbol{P}\overline{\boldsymbol{\xi}}_{k+N|k} \tag{24}$$

where N is the prediction horizon, $\overline{\boldsymbol{\xi}}_{k+i|k}$ and $\overline{\boldsymbol{\tau}}_{k+i|k}$ are the ith predicted state error and input obtained at time instant k.

The constrained optimization problem is then formulated as follows:

$$\begin{cases} \overline{\boldsymbol{v}}_{k+1} = \boldsymbol{A}(\overline{\boldsymbol{v}}_k)\overline{\boldsymbol{v}}_k + \boldsymbol{B}\overline{\boldsymbol{\tau}}_k \quad 0 \le i \le N-1 \\ \overline{\boldsymbol{\xi}}_{k|k} = \overline{\boldsymbol{\xi}}_k \\ \overline{\boldsymbol{\xi}}_{k+i|k} \in \overline{\mathbf{E}} \quad 0 \le i \le N-1 \\ \overline{\boldsymbol{\tau}}_{k+i|k} \in \overline{\mathbf{U}} \quad 0 \le i \le N-1 \\ \overline{\boldsymbol{\xi}}_{k+N|k} \in \boldsymbol{\Omega}(\varepsilon) \end{cases} \tag{25}$$

where $\boldsymbol{\Omega}(\varepsilon)$ is the terminal error constraint set.

3.2. Constraints and Control Input Modification

Based on modeling and analysis of rudder stuck faults in Section 2.3 and the construction of the controller without faults in Section 3.1, the FTMPC controller is built in this subsection. The fault term will be decoupled from the nominal vector, establishing the cost function of the new controller. Meanwhile, the input constraint set is updated.

When there is faulty rudder at time k, nominal control effort vector is transformed from $\overline{\boldsymbol{\Theta}}_{\boldsymbol{k}}$ to $\overline{\boldsymbol{\Theta}}_{\boldsymbol{k},f}$. The cost function Equation (24) is further derived as:

$$\begin{aligned} \boldsymbol{J} &= \sum_{i=0}^{N-1} \frac{1}{2}\overline{\boldsymbol{\xi}}_{k+i|k}^{\mathrm{T}}\boldsymbol{Q}\overline{\boldsymbol{\xi}}_{k+i|k} + \frac{1}{2}\overline{\boldsymbol{\tau}}_{k+i|k}^{\mathrm{T}}\boldsymbol{R}\overline{\boldsymbol{\tau}}_{k+i|k} + \frac{1}{2}\overline{\boldsymbol{\xi}}_{k+N|k}^{\mathrm{T}}\boldsymbol{P}\overline{\boldsymbol{\xi}}_{k+N|k} \\ &= \sum_{i=0}^{N-1} \frac{1}{2}\overline{\boldsymbol{\xi}}_{k+i|k}^{\mathrm{T}}\boldsymbol{Q}\overline{\boldsymbol{\xi}}_{k+i|k} + \frac{1}{2}\left(\overline{\boldsymbol{\tau}}_{k+i|k,f} + \overline{\boldsymbol{\tau}}_{k+i|k,c}\right)^{\mathrm{T}}\boldsymbol{R}\left(\overline{\boldsymbol{\tau}}_{k+i|k,f} + \overline{\boldsymbol{\tau}}_{k+i|k,c}\right) + \frac{1}{2}\overline{\boldsymbol{\xi}}_{k+N|k}^{\mathrm{T}}\boldsymbol{P}\overline{\boldsymbol{\xi}}_{k+N|k} \\ &= \sum_{i=0}^{N-1} \frac{1}{2}\overline{\boldsymbol{\xi}}_{k+i|k}^{\mathrm{T}}\boldsymbol{Q}\overline{\boldsymbol{\xi}}_{k+i|k} + \frac{1}{2}\overline{\boldsymbol{\tau}}_{k+i|k,f}^{\mathrm{T}}\boldsymbol{R}\overline{\boldsymbol{\tau}}_{k+i|k,f} + \frac{1}{2}\overline{\boldsymbol{\xi}}_{k+N|k}^{\mathrm{T}}\boldsymbol{P}\overline{\boldsymbol{\xi}}_{k+N|k} \\ &+ \frac{1}{2}\overline{\boldsymbol{\tau}}_{k+i|k,c}^{\mathrm{T}}\boldsymbol{R}\overline{\boldsymbol{\tau}}_{k+i|k,f} + \frac{1}{2}\overline{\boldsymbol{\tau}}_{k+i|k,f}^{\mathrm{T}}\boldsymbol{R}\overline{\boldsymbol{\tau}}_{k+i|k,c} + \frac{1}{2}\overline{\boldsymbol{\tau}}_{k+i|k,c}^{\mathrm{T}}\boldsymbol{R}\overline{\boldsymbol{\tau}}_{k+i|k,c} \\ &\ge \sum_{i=0}^{N-1} \frac{1}{2}\overline{\boldsymbol{\xi}}_{k+i|k}^{\mathrm{T}}\boldsymbol{Q}\overline{\boldsymbol{\xi}}_{k+i|k} + \frac{1}{2}\overline{\boldsymbol{\tau}}_{k+i|k,f}^{\mathrm{T}}\boldsymbol{R}\overline{\boldsymbol{\tau}}_{k+i|k,f} + \frac{1}{2}\overline{\boldsymbol{\xi}}_{k+N|k}^{\mathrm{T}}\boldsymbol{P}\overline{\boldsymbol{\xi}}_{k+N|k} \end{aligned} \tag{26}$$

Minimizing the cost function $\boldsymbol{J}$ as defined in Equation (24) is equivalent to minimizing $\boldsymbol{J}_f$, which can be expressed as follows:

$$\begin{aligned}\boldsymbol{J}_f &= \sum_{i=0}^{N-1} \frac{1}{2}\overline{\boldsymbol{\xi}}_{k+i|k}^{\mathrm{T}}\boldsymbol{Q}\overline{\boldsymbol{\xi}}_{k+i|k} + \frac{1}{2}\overline{\boldsymbol{\tau}}_{k+i|k,f}^{\mathrm{T}}\boldsymbol{R}\overline{\boldsymbol{\tau}}_{k+i|k,f} + \frac{1}{2}\overline{\boldsymbol{\xi}}_{k+N|k}^{\mathrm{T}}\boldsymbol{P}\overline{\boldsymbol{\xi}}_{k+N|k} \\ &= \sum_{i=0}^{N-1} \frac{1}{2}\overline{\boldsymbol{\xi}}_{k+i|k}^{\mathrm{T}}\boldsymbol{Q}\overline{\boldsymbol{\xi}}_{k+i|k} + \frac{1}{2}\left(\boldsymbol{B}_{\tau,f}\overline{\boldsymbol{\Theta}}_{k+i|k,f}\right)^{\mathrm{T}}\boldsymbol{R}\left(\boldsymbol{B}_{\tau,f}\overline{\boldsymbol{\Theta}}_{k+i|k,f}\right) + \frac{1}{2}\overline{\boldsymbol{\xi}}_{k+N|k}^{\mathrm{T}}\boldsymbol{P}\overline{\boldsymbol{\xi}}_{k+N|k} \\ &= \sum_{i=0}^{N-1} \frac{1}{2}\overline{\boldsymbol{\xi}}_{k+i|k}^{\mathrm{T}}\boldsymbol{Q}\overline{\boldsymbol{\xi}}_{k+i|k} + \frac{1}{2}\overline{\boldsymbol{\Theta}}_{k+i|k,f}^{\mathrm{T}}\boldsymbol{B}_{\tau,f}^{\mathrm{T}}\boldsymbol{R}\boldsymbol{B}_{\tau,f}\overline{\boldsymbol{\Theta}}_{k+i|k,f} + \frac{1}{2}\overline{\boldsymbol{\xi}}_{k+N|k}^{\mathrm{T}}\boldsymbol{P}\overline{\boldsymbol{\xi}}_{k+N|k} \\ &= \sum_{i=0}^{N-1} \frac{1}{2}\overline{\boldsymbol{\xi}}_{k+i|k}^{\mathrm{T}}\boldsymbol{Q}\overline{\boldsymbol{\xi}}_{k+i|k} + \frac{1}{2}\overline{\boldsymbol{\Theta}}_{k+i|k,f}^{\mathrm{T}}\boldsymbol{R}_{\tau}\overline{\boldsymbol{\Theta}}_{k+i|k,f} + \frac{1}{2}\overline{\boldsymbol{\xi}}_{k+N|k}^{\mathrm{T}}\boldsymbol{P}\overline{\boldsymbol{\xi}}_{k+N|k}\end{aligned} \tag{27}$$

where $\boldsymbol{R}_{\tau} = \boldsymbol{B}_{\tau,f}^{\mathrm{T}}\boldsymbol{R}\boldsymbol{B}_{\tau,f}$. The control input vector $\overline{\boldsymbol{\Theta}}_{k,f} = \left[\overline{T}_{1,k} \quad \overline{T}_{2,k}\right]^{T}$ when fault conditions are satisfied is within the new fault constraint set of actions $\overline{\boldsymbol{\Xi}}_f$.

$$\overline{\boldsymbol{\Theta}}_{k+i|k,f} \in \overline{\boldsymbol{\Xi}}_f \tag{28}$$

Through the above fault analysis and constraint transformation, the FTMPC controller of the AUV under rudder stuck faults is reconfigured as follows:

$$\min_{\overline{\boldsymbol{\Theta}}_{k:k+N-1|k,f}} \boldsymbol{J}_f \tag{29}$$

subject to:

$$\begin{gathered}\overline{\boldsymbol{v}}_{k+1} = \boldsymbol{A}(\overline{\boldsymbol{v}}_k)\overline{\boldsymbol{v}}_k + \boldsymbol{B}\overline{\boldsymbol{\tau}}_k \quad 0 \le i \le N-1 \\ \overline{\boldsymbol{\xi}}_{k|k} = \overline{\boldsymbol{\xi}}_k \\ \overline{\boldsymbol{\xi}}_{k+i|k} \in \overline{\mathbf{E}} \quad 0 \le i \le N-1 \\ \overline{\boldsymbol{\Theta}}_{\boldsymbol{k}+\mathrm{i}|\boldsymbol{k},f} \in \overline{\boldsymbol{\Xi}}_f \quad 0 \le i \le N-1 \\ \overline{\boldsymbol{\xi}}_{k+N|k} \in \boldsymbol{\Omega}(\varepsilon)\end{gathered} \tag{30}$$

where $\overline{\boldsymbol{\Xi}}_f$ is the constraint set of control efforts under rudder stuck faults, and other variables are defined similarly to Equations (24) and (25).

3.3. Feasibility and Asymptotic Stability Analysis

Due to the repeated solution of the optimization problem given by Equation (29), we need its feasibility at each time instant. Feasibility of the optimization problem means that there exists at least one (not necessarily optimal) solution such that the input constraint, state constraint, and terminal constraint are satisfied.

In order to show the recursive feasibility by using the induction principle, we assume that for the system with state $\overline{\boldsymbol{\xi}}_k$ at initial time k, the optimization problem in (29) has a solution.

First, a feasible control trajectory candidate at time $k+1$ is established by using the optimal control input sequence at k as

$$\overline{\boldsymbol{\Theta}}_{k+1+i|k+1,f} = \begin{cases} \overline{\boldsymbol{\Theta}}^{*}_{k+i+1|k,f} & i = 0, 1, \cdots, N-2 \\ \boldsymbol{B}_{\tau,f}^{+}\left(\boldsymbol{K}_f\overline{\boldsymbol{\xi}}^{*}_{k+N|k} - \overline{\boldsymbol{\tau}}_c\right) & i = N-1 \end{cases} \tag{31}$$

where $\boldsymbol{B}_{\tau,f}^{+}$ denotes the generalized inverse matrix of $\boldsymbol{B}_{\tau,f}$.

To prove it is a feasible solution of (29) at $k+1$, we show it can accommodate the input constraint, the state constraint, and the terminal constraint.

1. $\overline{\boldsymbol{\Theta}}_{k+1+i|k+1,f} \in \overline{\boldsymbol{\Xi}}_f$: it follows from the feasibility of $\overline{\boldsymbol{\Theta}}^{*}_{k+i+1|k,f}, i = 1, 2, \cdots N-1$ and the fact that $\boldsymbol{K}_f\overline{\boldsymbol{\xi}}^{*}_{k+N|k} \in \overline{\boldsymbol{\Xi}}_f$.

2. $\overline{\xi}_{k+1+i|k+1} \in \overline{\mathbf{E}}$, $i = 1, 2, \cdots, N-1$: Since the optimization problem is feasible at k, we have $\overline{\xi}^*_{k+i|k} \in \overline{\mathbf{E}}$, $i = 0, 2, \cdots, N-1$. Due to the expression of $\overline{\Theta}_{k+1+i|k+1,f}$, i = 0,1, $\cdots N-1$ in (31), there is $\overline{\xi}_{k+1+i|k+1} = \overline{\xi}^*_{k+i+1|k}$, $i = 0, 2, \cdots, N-1$. Therefore, the state constraint is satisfied.
3. $\overline{\xi}_{k+1+N|k+1} \in \boldsymbol{\Omega}(\varepsilon)$: Since the optimization problem is feasible at k, we know that $\overline{\xi}_{k+N|k+1} = \overline{\xi}^*_{k+N|k} \in \boldsymbol{\Omega}(\varepsilon)$. By using Lemma 1 (1), it is noted that the terminal set is a control invariant set under the feedback control law $\overline{\tau}_k = \boldsymbol{K}_f \boldsymbol{\xi}_k$. Therefore, by employing $\overline{\boldsymbol{\Theta}}_{k+1+i|k+1,f} = \boldsymbol{B}^+_{\tau,f}\left(\boldsymbol{K}_f \overline{\xi}^*_{k+N|k} - \overline{\tau}_c\right) = \boldsymbol{B}^+_{\tau,f}\left(\boldsymbol{K}_f \overline{\xi}_{k+N|k+1} - \overline{\tau}_c\right)$, it can be ensured that $\overline{\xi}_{k+1+N|k+1} \in \Omega(\varepsilon)$ is satisfied.

By combining the above 1–3, we have proved that (30) is a feasible solution of (29) at $k+1$. By deduction, if the optimization problem is feasible at 0. It will be feasible at every time instant, which is referred to as the recursive feasibility.

The asymptotic stability of the nominal tracking error system will be proved by showing that the optimal value function is decreasing.

To begin with, for time instant k, the optimal value function is given by

$$V^0_k = \sum_{i=0}^{N-1} \frac{1}{2} \overline{\xi}^*_{k+i|k}{}^T \boldsymbol{Q} \overline{\xi}^*{}_{k+i|k} + \frac{1}{2} \overline{\Theta}^*_{k+1|k,f}{}^T \boldsymbol{R}_\tau \overline{\Theta}^*{}_{k+1|k,f} + \frac{1}{2} \overline{\xi}^*_{k+N|k}{}^T \boldsymbol{P} \overline{\xi}^*{}_{k+N|k} \tag{32}$$

Additionally, for time instant $k+1$, the objective function by using the candidate control input sequence (31) is calculated as

$$\begin{aligned}
V_{k+1} &= \sum_{i=0}^{N-1} \frac{1}{2} \overline{\xi}^T_{k+1+i|k+1} \boldsymbol{Q} \overline{\xi}_{k+1+i|k+1} + \frac{1}{2} \overline{\Theta}^T_{k+1+i|k+1,f} \boldsymbol{R}_\tau \overline{\Theta}_{k+1+i|k+1,f} + \frac{1}{2} \overline{\xi}^T_{k+1+N|k+1} \boldsymbol{P} \overline{\xi}_{k+1+N|k+1} \\
&= \sum_{i=1}^{N-1} \frac{1}{2} \overline{\xi}^*_{k+i|k}{}^T \boldsymbol{Q} \overline{\xi}^*_{k+i|k} + \frac{1}{2} \overline{\Theta}^T_{k+i|k,f} \boldsymbol{R}_\tau \overline{\Theta}_{k+i|k,f} + \frac{1}{2} \overline{\xi}^*_{k+N|k}{}^T \boldsymbol{Q} \overline{\xi}^*_{k+N|k} \\
&+ \frac{1}{2} \left(\boldsymbol{B}^+_{\tau,f} \left(\boldsymbol{K}_f \overline{\xi}^*_{k+N|k} - \overline{\tau}_c \right) \right)^T \boldsymbol{R}_\tau \left(\boldsymbol{B}^+_{\tau,f} \left(\boldsymbol{K}_f \overline{\xi}^*_{k+N|k} - \overline{\tau}_c \right) \right) + \frac{1}{2} (\boldsymbol{A}_{\boldsymbol{K}_f} \overline{\xi}^*_{k+N|k})^T \boldsymbol{P} (\boldsymbol{A}_{\boldsymbol{K}_f} \overline{\xi}^*_{k+N|k}) \\
&\leq \sum_{i=1}^{N-1} \frac{1}{2} \overline{\xi}^*_{k+i|k}{}^T \boldsymbol{Q} \overline{\xi}^*_{k+i|k} + \frac{1}{2} \overline{\Theta}^T_{k+i|k,f} \boldsymbol{R}_\tau \overline{\Theta}_{k+i|k,f} + \frac{1}{2} \overline{\xi}^*_{k+N|k}{}^T \boldsymbol{Q} \overline{\xi}^*_{k+N|k} \\
&+ \frac{1}{2} \left(\boldsymbol{K}_f \overline{\xi}^*_{k+N|k} \right)^T \boldsymbol{R} \left(\boldsymbol{K}_f \overline{\xi}^*_{k+N|k} \right) + \frac{1}{2} (\boldsymbol{A}_{\boldsymbol{K}_f} \overline{\xi}^*_{k+N|k})^T \boldsymbol{P} (\boldsymbol{A}_{\boldsymbol{K}_f} \overline{\xi}^*_{k+N|k})
\end{aligned} \tag{33}$$

Further, $\widetilde{V}_{k+1}$ is defined as follows

$$\begin{aligned}
\widetilde{V}_{k+1} = &\sum_{i=1}^{N-1} \frac{1}{2} \overline{\xi}^*_{k+i|k}{}^T \boldsymbol{Q} \overline{\xi}^*_{k+i|k} + \frac{1}{2} \overline{\Theta}^T_{k+i|k,f} \boldsymbol{R}_\tau \overline{\Theta}_{k+i|k,f} + \frac{1}{2} \overline{\xi}^*_{k+N|k}{}^T \boldsymbol{Q} \overline{\xi}^*_{k+N|k} \\
&+ \frac{1}{2} \left(\boldsymbol{K}_f \overline{\xi}^*_{k+N|k} \right)^T \boldsymbol{R} \left(\boldsymbol{K}_f \overline{\xi}^*_{k+N|k} \right) + \frac{1}{2} (\boldsymbol{A}_{\boldsymbol{K}_f} \overline{\xi}^*_{k+N|k})^T \boldsymbol{P} (\boldsymbol{A}_{\boldsymbol{K}_f} \overline{\xi}^*_{k+N|k})
\end{aligned} \tag{34}$$

Therefore, we have

$$\begin{aligned}
&\widetilde{V}_{k+1} - V^0_k \\
&= V_f(\boldsymbol{A}_{\boldsymbol{K}_f} \overline{\xi}^*_{k+N|k}) - V_f(\overline{\xi}^*_{k+N|k}) + \tfrac{1}{2} \overline{\xi}^*_{k+N|k}{}^T \boldsymbol{Q}_{K_f} \overline{\xi}^*_{k+N|k} - \tfrac{1}{2} \overline{\xi}_{k|k}{}^T \boldsymbol{Q} \overline{\xi}_{k|k} - \overline{\boldsymbol{\Theta}}^*_{k|k}{}^T \boldsymbol{R}_\tau \overline{\boldsymbol{\Theta}}^*_{k|k}
\end{aligned} \tag{35}$$

Then by using Lemma 1 (2), we can further obtain

$$\widetilde{V}_{k+1} - V^0_k = -\frac{1}{2} \overline{\xi}_{k|k}{}^T \boldsymbol{Q} \overline{\xi}_{k|k} - \frac{1}{2} \overline{\boldsymbol{\Theta}}^*_{k|k}{}^T \boldsymbol{R}_\tau \overline{\boldsymbol{\Theta}}^*_{k|k} \leq 0 \tag{36}$$

Because (31) is not necessarily the optimal solution for (29) at $k+1$, the optimal value function at $k+1$ satisfies

$$V_{k+1}^0 - V_k^0 \leq V_{k+1} - V_k^0 \leq \widetilde{V}_{k+1} - V_k^0 \leq 0 \tag{37}$$

Therefore, the optimal value function is decreasing. Equation (32) can serve as a Lyapunov function, and the nominal error system is asymptotic stability.

Finally, by combing the convergence results of $\overline{\boldsymbol{\xi}}_k$ and $\boldsymbol{e}_k$, it is confirmed that the actual tracking error $\boldsymbol{\xi}_k$ is ultimately bounded.

4. Simulation Validation

Simulation and analysis are conducted by the CasADi framework in this section. Three simulation scenarios are conducted to validate the effectiveness of the proposed method in achieving AUV heading control. Meanwhile, the fault of the AUV rudder is considered in simulation verification to validate the effectiveness of the designed FTMPC controller. In addition, the simulation results were compared with traditional MPC methods. To improve visualization and facilitate interpretation in certain plots, the angular values in the simulation results have been converted from radians to degrees.

The fully-actuated AUV model in this study is based on the public REMUS AUV model [29], and the detailed parameters of the AUV model are listed in Table 1.

Table 1. Main parameters of the AUV model.

Parameter	Value	Unit	Parameter	Value	Unit
m	30.5	kg	$N_{r\|r\|}$	-131	Kg m^2/rad^2
$X_{\dot{u}}$	-0.93	kg	L_1	0.67	m
$Y_{\dot{v}}$	-35.5	kg	L_2	0.67	m
$N_{\dot{r}}$	-4.88	kg m^2	$T_{1,2,\max}$	50	N
X_u	-7.8	kg/s	$T_{1,2,\min}$	-50	N
Y_v	-262	kg/s	$T_{3,\max}$	150	N
N_r	-188	kg m^2/(rad s)	$T_{3,\min}$	0	N
$X_{u\|u\|}$	-3.9	kg/m	$\delta_{R,\max}$	$\pi/6$	Rad
$Y_{v\|v\|}$	-131	kg/m	$\delta_{R,\min}$	$-\pi/6$	Rad

4.1. Simulation Results of Fixed Heading Control

In this simulation scenario, the main simulation parameters are set: initial state of the AUV is $\eta_0 = [0 \quad 0 \quad 0]^T$ and $v_0 = [0 \quad 0 \quad 0]^T$, $T = 0.01$ s denotes the sampling period; $N = 10$ is the prediction horizon of MPC; the target heading angle is $\psi = 0^\circ$; the auxiliary thrust of the thrusters is limited within a certain range as Equation (13); the rudder angle is constrained as in Equation (6); the thrust force of the main thruster is set to a constant, $T_m = 50$ N. In order to simulate the underwater environment of the AUV motion more accurately, we included undefined disturbance factors in Equation (3) as

$$\begin{cases} d_X = 0.5\sin(0.25\pi t) \\ d_Y = 0.3\cos(0.2\pi t) \\ d_N = 0.5\sin(0.5\pi t) \end{cases} \tag{38}$$

Set the fault condition to a rudder stuck fault where the rudder is stuck at 15 degrees at the 1.5th second during the driving process, i.e., $\alpha = 15^\circ$.

The motion trajectory of AUVs using different control strategies is shown in Figure 4a. Figure 4b shows the variation of heading angles. Figure 5 shows the variations of position

error and heading angle error. Meanwhile, the variation of control inputs, including two auxiliary thrusters, one main thruster, and rudder angle, is demonstrated in Figure 6.

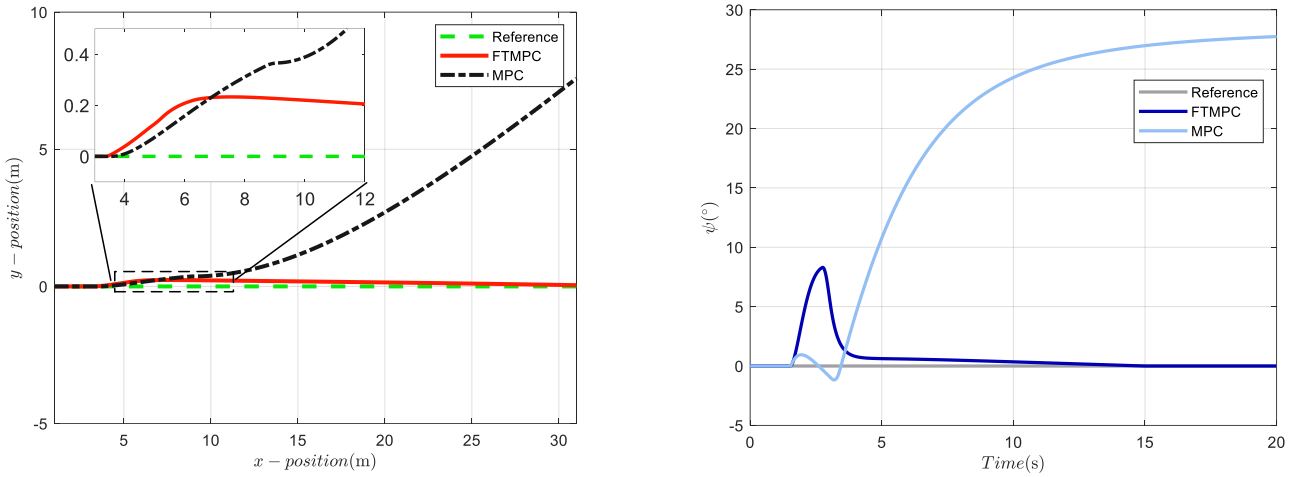

(**a**) (**b**)

Figure 4. Fixed heading control simulation results in the first case: (**a**) Motion trajectory; (**b**) variation of heading angle.

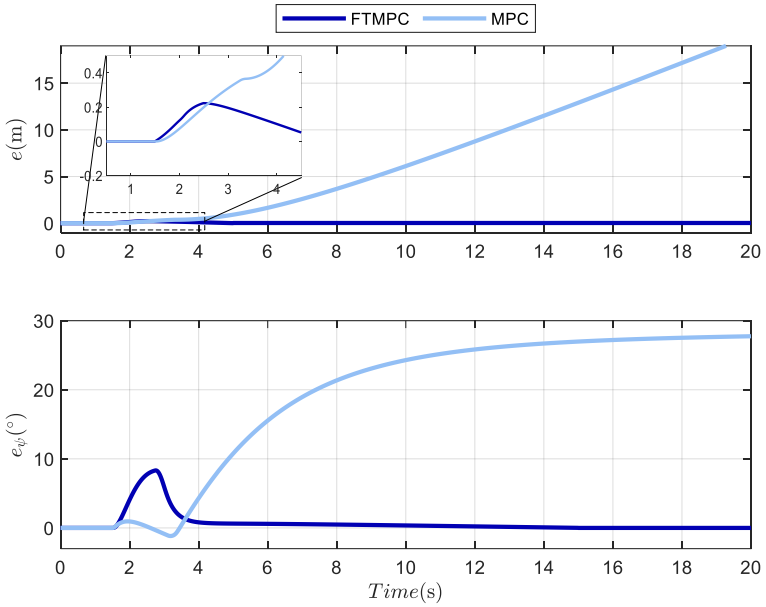

Figure 5. Position and heading angle error in the first case. The position error e represents the Euclidean distance between the actual position and the reference position. The heading error e_ψ represents the difference between the actual heading angle and the reference heading angle.

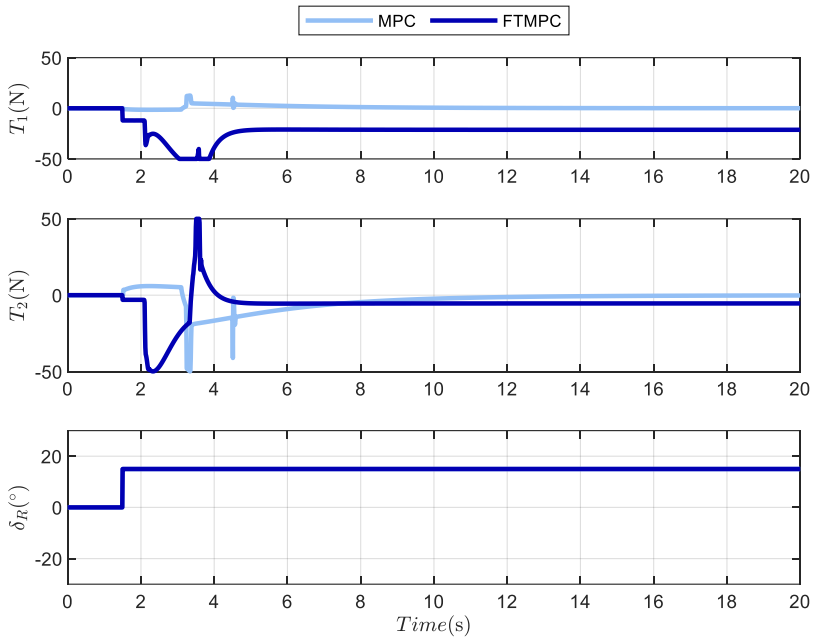

Figure 6. Control efforts in the first case include thrust forces of the auxiliary thrusters (#1 and #2) and vertical rudder angle. The rudder stuck fault occurs around 1.5 s.

Based on the motion path under fault-free conditions, the effect of FTMPC is observed. In this simulation, the rudder stuck fault occurs at 1.5 s, and the AUV using FTMPC is adjusted promptly after a small deviation from the target heading angle. However, the AUV trajectory using traditional MPC deviates from the normal heading angle.

As shown in Figure 4b, under fault-free conditions, the AUV with MPC achieves a heading control of 0°. The heading angle of the AUV using FTMPC is quickly deflected after the rudder fault occurs and reaches its maximum value of 8° around 2.7 s. Meanwhile, the heading angle of the AUV using traditional MPC also deviates and rapidly diverges. On the contrary, under the control of FTMPC, the heading angle of the AUV is adjusted and ultimately converges to 0°.

Figure 5 illustrates the variations in position error and heading angle error between the actual trajectory and the reference trajectory of the AUV. At approximately 1.5 s, a fault occurs, leading to a maximum deviation of 0.4 m in the y-position for the AUV employing the proposed method, alongside a corresponding change in the heading angle. Despite this, the proposed control method adjusts the AUV to the desired heading angle within approximately 3 s. In contrast, AUV utilizing conventional MPC exhibits significant divergence in its global y-position and heading following the malfunction.

According to the variations of the control effort in Figure 6, when the fault occurs, the auxiliary thruster is required to continuously provide thrust to compensate for the torque changes caused by rudder faults. For the proposed controller, auxiliary thruster #1 reaches its maximum thrust of 50 N in the third second and stabilizes at around 20 N in the fifth second. The thrust of auxiliary thruster #2 continuously adjusts from the 2nd to the 4th second, reaches its peak at the 3.5th second, and then begins to decrease before gradually stabilizing.

4.2. Simulation Results of Heading Change Control

For heading change control of the AUV, the initial state is set as $\eta_0 = [0, 0, 0]^T$ and $v_0 = [0, 0, 0]^T$. $T = 0.01$ s denotes the sampling period; the prediction horizon of controller

is set to $N = 20$; the thrust force of the main thruster is $T_m = 70$ N; the target heading angle is

$$\psi_d = \begin{cases} 0^\circ & x \leq 55 \\ -90^\circ & x > 55 \end{cases} \tag{39}$$

In this case, set the fault condition to the rudder stuck at -10 degrees at the 9.5th second, i.e., $\alpha = -10^\circ$. In addition, the disturbance factors are designed in Equation (3) as

$$\begin{cases} d_X = 0.3\sin(0.3\pi t) \\ d_Y = 0.3\cos(0.3\pi t) \\ d_N = 0.2\sin(0.3\pi t) \end{cases} \tag{40}$$

The simulation results of heading change control are shown in Figure 7. In accordance with the data presented in the results, it is evident that when the rudder fault occurs, the deviation in both the position and the heading angle of the AUV which is operating under traditional MPC will experience further expansion. At the same time, it is also notable that the convergence speed of the AUV when employing the proposed controller has been reduced.

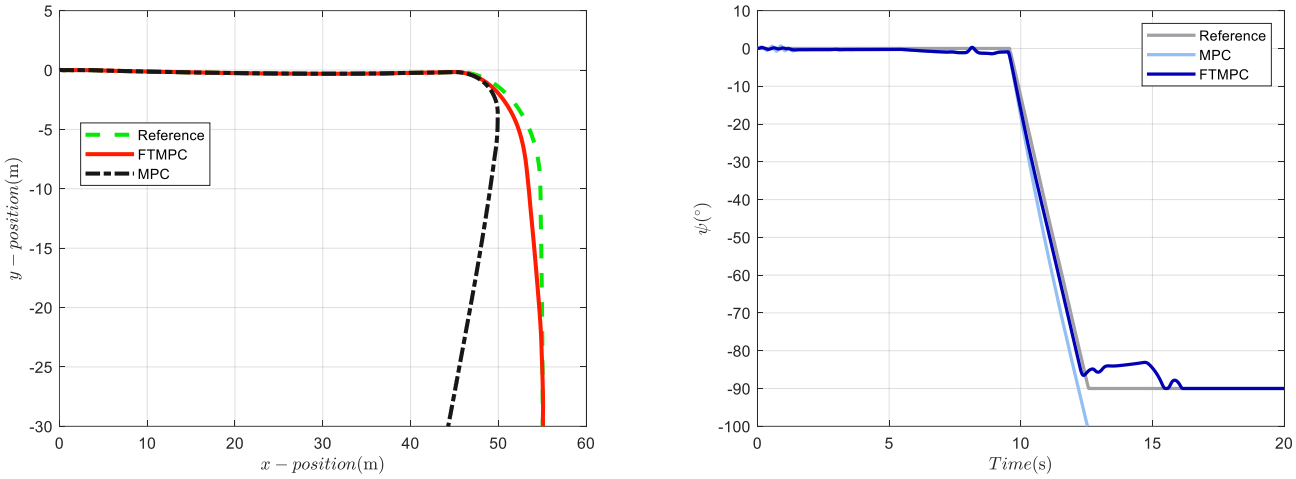

(**a**) (**b**)

Figure 7. Heading change control simulation results in the second case: (**a**) Motion trajectory; (**b**) variation of heading angle.

Figure 7a shows the global motion trajectory of the AUV. AUVs using both methods can smoothly achieve heading control before the rudder fault occurs. After changing the reference heading angle, the AUV using the proposed method performs a turning action at approximately 45 m to achieve fault tolerant control. At approximately $y = -25$ m, tracking of position and heading is achieved using an AUV with FTMPC. After a fault occurs, the yaw angle deviation of the AUV using traditional MPC is generated starting from $x = 45$ m.

As shown in Figure 7b, the heading angle of the AUV using the proposed method converges to the reference heading angle within approximately 7 s after the fault. Starting from the 9th second, both AUVs begin to move with a reference heading of -90°as the target. Due to the presence of faults, the heading angle of the traditional MPC AUV is -100° in the 12th second and continued to diverge thereafter. The heading angle of the AUV using the proposed method is -83° at the 14th second and converges to -90° around the 17th second.

According to Figure 8, within the first 9 s, the maximum heading angle error is $-1.5°$ at around 8.5 s. From around the 12th second, the position error of the AUV using FTMPC is approximately 2 m, after which the error gradually decreases and eventually converges to 0. The position error converges to 0 around the 17th second.

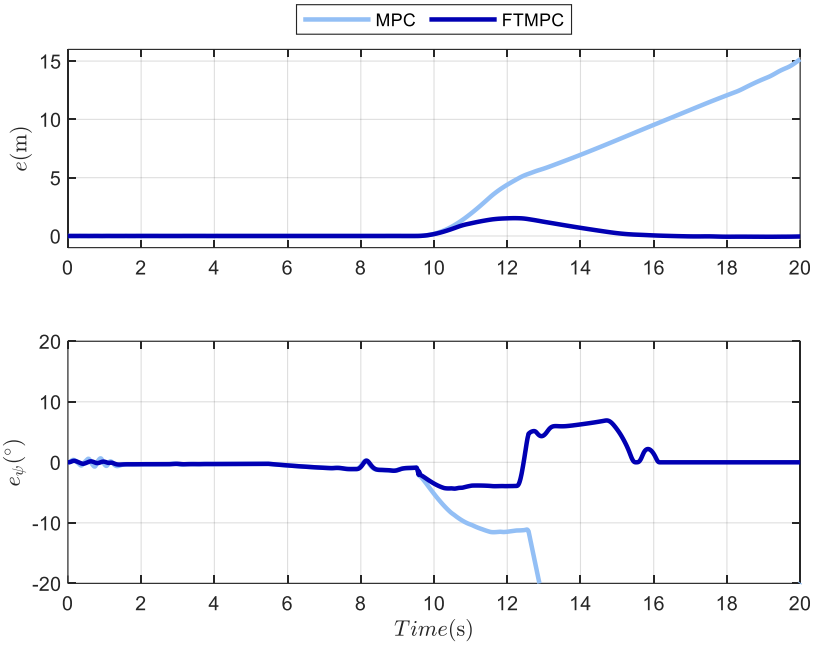

Figure 8. Position and heading angle error in the second case. The position error e represents the Euclidean distance between the actual position and the reference position. The heading error e_ψ represents the difference between the actual heading angle and the reference heading angle.

In Figure 9, the variations of the control input value are shown. Initially, the control input differences between the two controllers are minimal. However, between the 8th and 10th seconds, the AUV's vertical rudder becomes stuck at a fault angle of $-10°$. The traditional MPC lacks a fault response strategy, preventing it from leveraging auxiliary thrusters to adjust the AUV's heading angle.

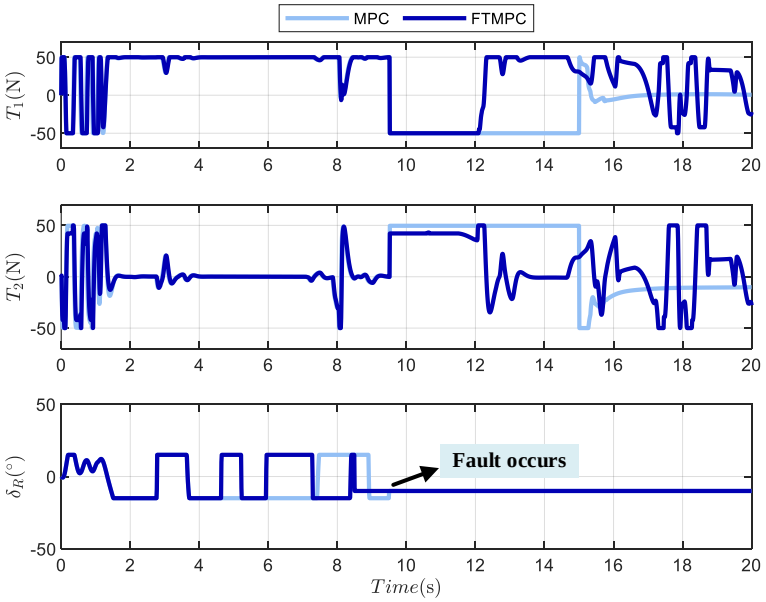

Figure 9. Control efforts in the second case include thrust forces of the auxiliary thrusters (#1 and #2) and vertical rudder angle. The rudder stuck fault occurs around 9.5 s.

4.3. Simulation Results of Z-Shaped Tracking and Heading Change Control

This subsection introduces a simulation study to evaluate the effectiveness of the proposed fault-tolerant MPC method under a Z-shaped trajectory tracking scenario. The aim is to verify its performance in managing sharp heading changes and ensuring stability in the presence of faults. The backstepping fault-tolerant control (BFTC) method detailed in Ref. [4] will be incorporated into the simulations to facilitate a comparative evaluation.

The primary simulation parameters are configured as follows: $\eta_0 = [0, 0, -\pi/2]^T$ and $v_0 = [0, 0, 0]^T$; the thrust force of the main thruster is $T_m = 90$ N; the prediction horizon of controller is set to $N = 30$; the disturbance settings are identical to those in case 2. The rudder stuck fault occurs at the 20th second and $\alpha = 10^\circ$.

The simulation results of Z-shaped tracking and heading change control are shown in Figures 10–12.

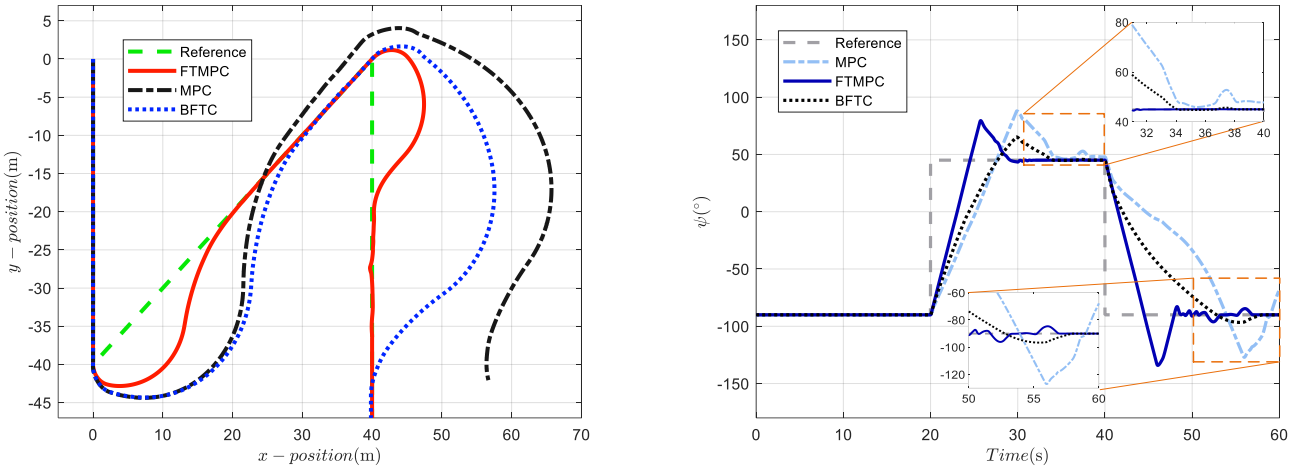

(**a**) (**b**)

Figure 10. Simulation results of Z-shaped tracking and heading change control: (**a**) Motion trajectory; (**b**) Variation of heading angle.

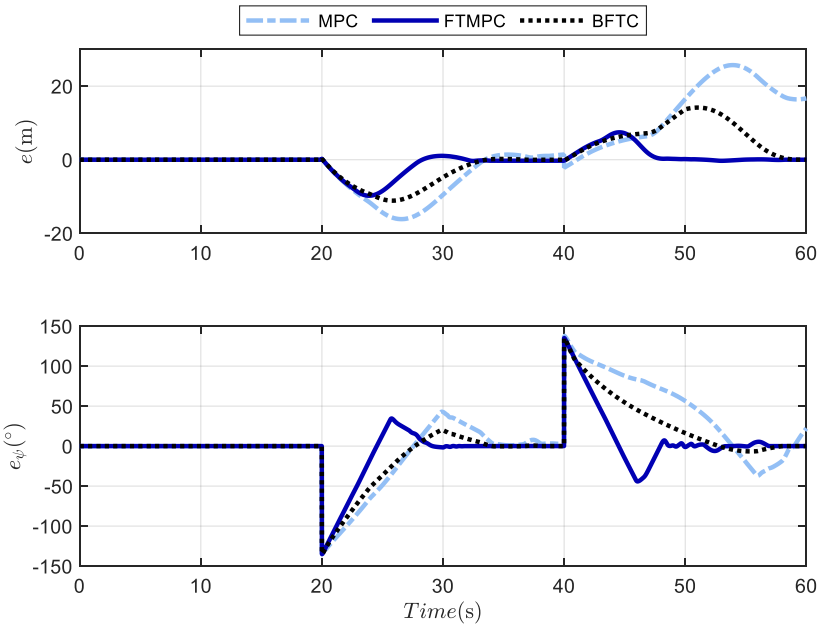

Figure 11. Position and heading angle error in the third case. The position error e represents the Euclidean distance between the actual position and the reference position. The heading error e_ψ represents the difference between the actual heading angle and the reference heading angle.

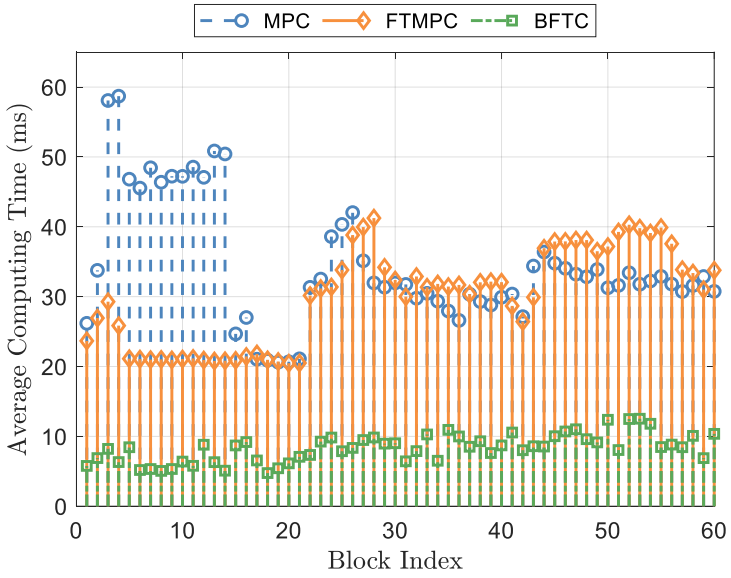

Figure 12. The stem plots of the computation time. To enhance data clarity and conciseness, the stem plot is generated using block-averaged computation times, with each block representing the mean of 100 iterations.

The motion trajectories and heading angle variations of the AUV under stuck rudder faults with different control methods are depicted in Figure 10. The conventional MPC demonstrates limited effectiveness in handling the stuck rudder fault, failing to maintain stable control of the AUV. In contrast, both the BFTC and the proposed fault-tolerant control method enable effective fault compensation. Notably, the AUV using the proposed FTMPC achieves faster convergence and reduced tracking errors compared to the BFTC.

As illustrated in Figure 11, the conventional MPC does not achieve convergence of the position and heading errors under fault conditions. In contrast, the fault-tolerant method demonstrates better fault handling capabilities, despite a slower convergence rate due to abrupt heading changes. Notably, the maximum position error observed with the FTMPC method is -9.8 m, compared to 16.7 m for the BFTC method, indicating a marked improvement in trajectory accuracy.

Additionally, the optimization time of the MPC is analyzed, as depicted in Figure 12, which presents the stem plots of computation times for the different methods. Table 2 provides a summary of the performance indicators, including the average computation time and the MPC cost function for various fault-tolerant control strategies under rudder fault conditions. The results indicate that the computation times for MPC and FTMPC are comparable, while BFTC demonstrates superior computational efficiency.

Table 2. Performance indicators of different methods.

Indicators	MPC	FTMPC	BFTC
Average iteration time (ms)	34.26	30.30	8.35
Average cost value	3.19×10^5	2.45×10^5	-

5. Conclusions

This study presents a fault-tolerant model predictive control framework designed for fully-actuated AUVs. The proposed controller addresses the challenges related to rudder stuck faults while effectively managing actuator input saturation. By conducting a comprehensive analysis of the allocation mechanisms of thrusters and ruddeOKrs, fault models are developed and integrated into the control design as specific constraint sets. This

methodological integration ensures robust fault management and enhances the overall resilience of the AUV control system. In simulation scenarios, the AUV equipped with the proposed controller demonstrates markedly enhanced performance compared to conventional MPC. Specifically, the controller effectively compensates for torque imbalances caused by rudder stuck faults by modulating the auxiliary thruster, thereby ensuring stable and reliable operation. Simulation results validate the effectiveness of the proposed approach, demonstrating that the controller can handle rudder stuck faults, maintaining fault tolerance and system stability.

However, the computational intensity of MPC remains a limitation, potentially impacting real-time performance in complex operational environments. Despite this, the proposed approach provides critical technical support for AUVs in underwater missions, enabling stable operation during rudder stuck faults and reducing the risk of task failures, thus advancing the practical implementation of fault-tolerant control systems.

Future research efforts will concentrate on multiple crucial aspects.

1. We aim to incorporate a more diverse array of fault scenarios related to AUV actuators. Extensive simulations will be conducted to rigorously validate the proposed methodologies.
2. To improve the real-time performance of MPC, which is currently limited, we will explore model reduction and parallel computing. Model reduction will simplify the AUV model without losing critical accuracy, reducing computational load. Additionally, parallel computing will distribute MPC's complex tasks across multiple processors or cores.
3. We are committed to integrating the fault-tolerant MPC strategies into real-world AUV control systems. This step is crucial for facilitating the practical validation of their performance and robustness under actual operational conditions.

Author Contributions: Conceptualization, Y.C. and S.H.; methodology, Y.C. and S.H.; software, Y.C.; validation, J.G. and J.W.; formal analysis, J.W.; writing—original draft preparation, S.H. and L.L.; writing—review and editing, Y.C., J.G., J.W. and L.L.; funding acquisition, Y.C. All authors have read and agreed to the published version of the manuscript.

Funding: This work is supported in part by the National Natural Science Foundation of China under Grants of 52471347 and 52102469, in part by the Double First-Class Foundation under Grants of 0206022GH0202.

Institutional Review Board Statement: Not applicable.

Informed Consent Statement: Not applicable.

Data Availability Statement: Dataset available on request from the authors.

Conflicts of Interest: The authors declare no conflicts of interest.

References

1. Wen, T.; He, X.; Xu, G. Robust Trajectory Tracking and Control Allocation of X-Rudder AUV with Actuator Uncertainty. *Control Eng. Pract.* **2023**, *136*, 105535. [CrossRef]
2. Amin, A.A.; Hasan, K.M. A Review of Fault Tolerant Control Systems: Advancements and Applications. *Measurement* **2019**, *143*, 58–68. [CrossRef]
3. Liu, F.; Ma, Z.; Mu, B.; Duan, C.; Chen, R.; Qin, Y.; Pu, H.; Luo, J. Review on Fault-Tolerant Control of Unmanned Underwater Vehicles. *Ocean. Eng.* **2023**, *285*, 115471. [CrossRef]
4. Zhang, M.; Liu, X.; Wang, F. Backstepping Based Adaptive Region Tracking Fault Tolerant Control for Autonomous Underwater Vehicles. *J. Navig.* **2017**, *70*, 184–204. [CrossRef]

5. Rauber, J.G.; Dos Santos, C.H.F.; Chiella, A.C.B.; Motta, L.R.H. A Strategy for Thruster Fault-Tolerant Control Applied to an AUV. In Proceedings of the 2012 17th International Conference on Methods & Models in Automation & Robotics (MMAR), Miedzyzdroje, Poland, 27–30 August 2012; IEEE: Miedzyzdroje, Poland, 2012; pp. 184–189.
6. Chen, Y.; Gao, J.; Wang, Y.; Pan, G. Collision Avoidance Strategy for Unmanned Surface Vessel Considering Actuator Faults Using Kinodynamic Rapidly Exploring Random Tree-Smart and Radial Basis Function Neural Network-Based Model Predictive Control. *J. Mar. Sci. Eng.* **2023**, *11*, 1107. [CrossRef]
7. Liu, F.; Xu, D. Fault Localization and Fault-Tolerant Control for Rudders of AUVs. In Proceedings of the 2016 35th Chinese Control Conference (CCC), Chengdu, China, 27–29 July 2016; IEEE: Chengdu, China, 2016; pp. 6537–6541.
8. Chaos, D.; Moreno-Salinas, D.; Aranda, J. Fault-Tolerant Control for AUVs Using a Single Thruster. *IEEE Access* **2022**, *10*, 22123–22139. [CrossRef]
9. Tian, Q.; Wang, T.; Liu, B.; Ran, G. Thruster Fault Diagnostics and Fault Tolerant Control for Autonomous Underwater Vehicle with Ocean Currents. *Machines* **2022**, *10*, 582. [CrossRef]
10. Ping, X.; Hu, J.; Lin, T.; Ding, B.; Wang, P.; Li, Z. A Survey of Output Feedback Robust MPC for Linear Parameter Varying Systems. *IEEE/CAA J. Autom. Sin.* **2022**, *9*, 1717–1751. [CrossRef]
11. Zhao, H.; Zhu, D. UUV Trajectory Tracking Control with Fault Tolerant Based on MPC. In Proceedings of the 2020 Chinese Control And Decision Conference (CCDC), Hefei, China, 22–24 August 2020; IEEE: Hefei, China, 2020; pp. 2403–2408.
12. Zhang, H.; Zhu, D.; Liu, C.; Hu, Z. Tracking Fault-Tolerant Control Based on Model Predictive Control for Human Occupied Vehicle in Three-Dimensional Underwater Workspace. *Ocean. Eng.* **2022**, *249*, 110845. [CrossRef]
13. Valencia-Palomo, G.; Rossiter, J.A. Using Laguerre Functions to Improve Efficiency of Multi-Parametric Predictive Control. In Proceedings of the 2010 American Control Conference, Baltimore, MD, USA, 30 June–2 July 2010; IEEE: Baltimore, MD, USA, 2010; pp. 4731–4736.
14. Valencia-Palomo, G.; Rossiter, J.A. Novel Programmable Logic Controller Implementation of a Predictive Controller Based on Laguerre Functions and Multiparametric Solutions. *IET Control Theory Appl.* **2012**, *6*, 1003–1014. [CrossRef]
15. Wang, W.; Yan, J.; Wang, H.; Ge, H.; Zhu, Z.; Yang, G. Adaptive MPC Trajectory Tracking for AUV Based on Laguerre Function. *Ocean. Eng.* **2022**, *261*, 111870. [CrossRef]
16. Yan, Z.; Yan, J.; Cai, S.; Yu, Y.; Wu, Y. Robust MPC-Based Trajectory Tracking of Autonomous Underwater Vehicles with Model Uncertainty. *Ocean. Eng.* **2023**, *286*, 115617. [CrossRef]
17. Gong, P.; Yan, Z.; Zhang, W.; Tang, J. Trajectory Tracking Control for Autonomous Underwater Vehicles Based on Dual Closed-Loop of MPC with Uncertain Dynamics. *Ocean. Eng.* **2022**, *265*, 112697. [CrossRef]
18. Cui, Y.; Peng, L.; Li, H. Filtered Probabilistic Model Predictive Control-Based Reinforcement Learning for Unmanned Surface Vehicles. *IEEE Trans. Ind. Inf.* **2022**, *18*, 6950–6961. [CrossRef]
19. Gan, W.; Zhu, D.; Ji, D. QPSO-Model Predictive Control-Based Approach to Dynamic Trajectory Tracking Control for Unmanned Underwater Vehicles. *Ocean. Eng.* **2018**, *158*, 208–220. [CrossRef]
20. Zhang, Y.; Gao, J.; Chen, Y.; Bian, C.; Zhang, F.; Liang, Q. Adaptive Neural Network Control for Visual Docking of an Autonomous Underwater Vehicle Using Command Filtered Backstepping. *Intl J. Robust. Nonlinear* **2022**, *32*, 4716–4738. [CrossRef]
21. Gao, J.; Wu, P.; Yang, B.; Xia, F. Adaptive Neural Network Control for Visual Servoing of Underwater Vehicles with Pose Estimation. *J. Mar. Sci. Technol.* **2017**, *22*, 470–478. [CrossRef]
22. Gao, J.; Proctor, A.A.; Shi, Y.; Bradley, C. Hierarchical Model Predictive Image-Based Visual Servoing of Underwater Vehicles with Adaptive Neural Network Dynamic Control. *IEEE Trans. Cybern.* **2016**, *46*, 2323–2334. [CrossRef]
23. Van, M.; Ge, S.S. Adaptive Fuzzy Integral Sliding-Mode Control for Robust Fault-Tolerant Control of Robot Manipulators with Disturbance Observer. *IEEE Trans. Fuzzy Syst.* **2021**, *29*, 1284–1296. [CrossRef]
24. Sharifi, F.; Mirzaei, M.; Gordon, B.W.; Zhang, Y. Fault Tolerant Control of a Quadrotor UAV Using Sliding Mode Control. In Proceedings of the 2010 Conference on Control and Fault-Tolerant Systems (SysTol), Nice, France, 6–8 October 2010. [CrossRef]
25. Lv, T.; Zhou, J.; Wang, Y.; Gong, W.; Zhang, M. Sliding Mode Based Fault Tolerant Control for Autonomous Underwater Vehicle. *Ocean. Eng.* **2020**, *216*, 107855. [CrossRef]
26. Li, H.; Lin, X. Robust Finite-Time Fault-Tolerant Control for Dynamic Positioning of Ships via Nonsingular Fast Integral Terminal Sliding Mode Control. *Appl. Ocean. Res.* **2022**, *122*, 103126. [CrossRef]
27. Zheng, Y.; Liu, Z.; Liu, L. Robust MPC-Based Fault-Tolerant Control for Trajectory Tracking of Surface Vessel. *IEEE Access* **2018**, *6*, 14755–14763. [CrossRef]

28. Fossen, T.I.; Fjellstad, O.E. Nonlinear Modeling of Marine Vehicles in 6 Degrees of Freedom. *Mathematical Modelling of System.* **1995**, *1*, 17–27. [CrossRef]
29. Prestero, T. *Verification of a Six-Degree of Freedom Simulation Model for the REMUS Autonomous Underwater Vehicle*; Massachusetts Institute of Technology and Woods Hole Oceanographic Institution: Woods Hole, MA, USA, 2001.